Imaging of the scarred wave functions in chaotic quantum cavities

Y. Takagaki and K. H. Ploog
Paul-Drude-Institut für Festkörperelektronik, Hausvogteiplatz 5-7, 10117 Berlin, Germany
(Received 2 April 2004; revised manuscript received 18 May 2004; published 9 August 2004)

We numerically investigate the possibility of imaging the wave function scarring in chaotic quantum cavities using the conductance modifications induced by a scanning probe. Quantum cavities having mixed or chaotic underlying classical dynamics are examined. The modifications are shown to produce the electron probability distribution in a two-dimensional electron gas irrespective of the type of the underlying classical dynamics.

DOI: 10.1103/PhysRevB.70.073304 PACS number(s): 73.23.Ad, 05.45.Pq, 73.21.La

A technique to visualize the probability distribution in a two-dimensional electron gas (2DEG) in semiconductor heterostructures has been demonstrated in recent years.[1] The changes in the conductance of the 2DEG are measured when the electrostatic potential is altered locally by a biased scanning probe. The conductance modification is large when the probe is placed at the regions of large electronic probability densities.[2] Crook *et al.*[3] applied the technique to investigate the wave functions in so-called quantum billiards. The development of scarlike features in the mapped images when the external magnetic field was varied was attributed to the existence of stable classical orbits in the cavity.

In considering the plausibility of imaging the electronic wave functions in quantum billiards, it is important to make a rigorous distinction between chaotic and mixed dynamics.[4] An electron placed in an open chaotic cavity easily finds the exit to escape from the cavity. The probability of electrons staying in the cavity diminishes exponentially with time. The situation is different for mixed dynamics. The phase space of mixed dynamics is characterized by a hierarchical mixture of chaotic sea and regular orbits. Electron trajectories are attracted to be in the vicinity of the regular orbits. Electrons dwell in the cavity much longer than expected for chaotic dynamics. The "stickiness" is known to lead to a power-law distribution of the dwell time.[5] The conductance fluctuations in quantum cavities have been predicted to become fractal when the probability distributions obey a power-law behavior.[6] The quantum billiards studied by Crook *et al.*[3] belong to the latter case. The experiment can benefit from the stability of classical orbits in mixed dynamics. It is not obvious in the case of chaotic dynamics, where classical trajectories are altered dramatically even by a small perturbation, whether the probe-induced conductance change can faithfully mimic the true scar of the wave function in chaotic quantum cavities.[7]

In this paper, we numerically simulate the images expected by the scanned gate microscopy (SGM). We analyze the correlation between the constructed images and the probability distribution of the electron wave function when the underlying classical dynamics is altered between being chaotic and mixed. Similar simulations were performed by Mendoza and Schulz.[8] They dealt with quantum dots of sizes comparable with the Fermi wavelength λ_F. The conductance change produced, as expected, simple standing-wave patterns of low-lying quasi-zero-dimensional states.[9] The quantum cavities to be investigated below are much larger than λ_F.

We employ in our study three types of quantum cavities: a soft-wall cavity, a stadium cavity, and a square cavity having a short-range boundary disorder. The underlying classical dynamics in soft-wall cavities is mixed. The remaining two types of cavities are intended to realize chaotic dynamics. The quantum cavities are simulated using a tight-binding square lattice model having a lattice constant a. The quantum cavities are attached by two leads. The conductance G of the system is related to the transmission probabilities between the leads by the Landauer formula. The transmission coefficients are calculated using the lattice Green's-function method.

Let us first discuss SGM images obtained in soft-wall cavities. Our model confinement potential comprises of a flat bottom at the center of the cavity and soft walls given by two parabolas defined in the direction perpendicular to the cavity axis.[6,10] The dotted and thick solid lines in Fig. 1(b) show the boundary between the parabolas and the flat bottom and the cavity boundary at the Fermi level, respectively. The length and the width of the cavity are L and W, respectively. We assume $L=1.4W=160a$. In Fig. 1(a), we show the conductance of the soft-wall quantum cavity when the magnetic field B is varied for $L/\lambda_F=20$. Here, $\omega_c=eB/m$ is the cyclo-

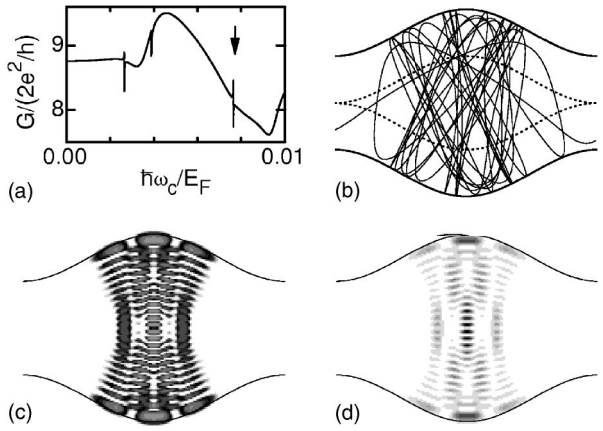

FIG. 1. (a) Magnetoconductance in a soft-wall cavity. The simulated scanned gate micrograph $\delta G(\mathbf{r})$ when $U=0.1t$ (c) and the local density-of-states $\rho(\mathbf{r})$ (d) are calculated at the transmission resonance peak indicated by the arrow. An example of the classical trajectory is shown in (b). The black and white regions in the gray scale in (c) correspond to $\delta G/(2e^2/h)\approx -0.80$ and 0.12, respectively. Darker regions represent larger ρ in (d).

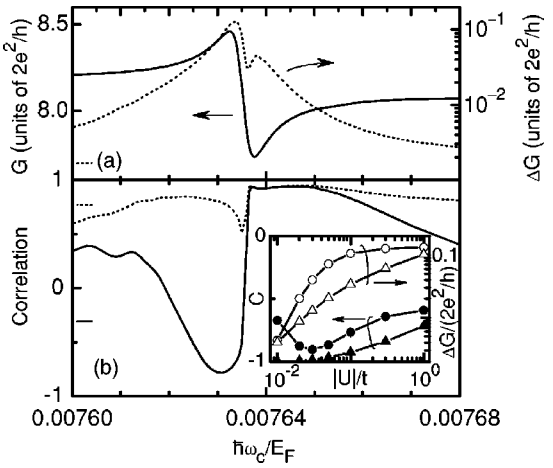

FIG. 2. (a) Conductance G in Fig. 1(a) with an expanded magnetic-field scale. The dotted line shows the absolute magnitude of the conductance change ΔG averaged in the cavity area when $U=0.1t$. (b) The correlations C and $\tilde{C}$ when $U=0.1t$ are shown by the solid and dotted lines, respectively. The horizontal bars indicate the values when $\hbar\omega_c/E_F=0.0065$. The inset shows C and ΔG when U is varied for the transmission resonance peak indicated by the arrow in Fig. 1(a). The circles and triangles are for $U>0$ and $U<0$, respectively.

tron angular frequency and E_F the Fermi energy. The magnetoconductance consists of a slow background and sharp transmission resonances. The wave function develops a pronounced nonuniformity at the resonances, which reveals the quasibound states responsible for the resonances. This scarlike feature is associated with the stable orbits in mixed dynamics and hence its origin is classical.[10,11]

We examine the SGM images obtained for the Fano-type transmission resonance indicated by the arrow in Fig. 1(a). The resonance is shown with an expanded magnetic-field scale in Fig. 2(a): a resonance peak and a resonance dip are combined with a small separation in the magnetic field. We plot in Fig. 1(d) the local density-of-states (LDOS) $\rho(\mathbf{r})=-\pi^{-1}\mathrm{Im}G^{+}(\mathbf{r},\mathbf{r};E_F)$ at the Fermi energy E_F, where $G^{+}(E)=(E-H+i\epsilon)^{-1}$ is the retarded Green's function with H being the Hamiltonian of the system. A typical classical trajectory attracted to a stable orbit is shown in Fig. 1(b). The resemblance between Figs. 1(b) and 1(d) is a manifestation of the classical origin of the scarlike feature. The scarlike pattern is essentially unchanged for the magnetic-field range in Fig. 2, as stable orbits hardly change with a slight shift in magnetic field. However, the wave function is increasingly delocalized when the magnetic field deviates from the transmission resonance. Away from transmission resonances, the wave function generally exhibits a weak scarlike pattern interwoven in an almost homogeneous background.

The simulated SGM image is shown in Fig. 1(c). Here, we plot the conductance change $\delta G(\mathbf{r};U)$ when the on-site potential at the lattice site $\mathbf{r}$ was increased by $U=0.1t$, where $t=\hbar^2/2ma^2$. The pattern in LDOS shown in Fig. 1(d) is well reproduced. Notice that the maximum conductance changes take place in Fig. 1(c) along contours encircling the peaks in LDOS. This originates from the somewhat excessive potential modulation. When U is reduced to be closer to zero, the positions of the maximum conductance changes almost coincide with the peaks in LDOS.

In order to quantitatively analyze the similarity between the SGM images and the pattern in LDOS, we evaluate a correlation which is defined as

$$C(U)=\frac{\int\delta G(\mathbf{r};U)\rho(\mathbf{r})d\mathbf{r}^2}{[\int\delta G(\mathbf{r};U)^2d\mathbf{r}^2\int\rho(\mathbf{r})^2d\mathbf{r}^2]^{1/2}}. \quad (1)$$

We show $C(U)$ by the solid line in Fig. 2(b). The correlation estimated in the above manner erroneously appears to be absent, even if the SGM images resemble the scarlike pattern in $\rho(\mathbf{r})$, when the domains of positive and negative local correlation occupy comparable areas. Therefore, $\delta G(\mathbf{r};U)$ in Eq. (1) has been replaced with its absolute magnitude for the dotted line in Fig. 2(b). The correlation for $|\delta G|$, which we denote as $\tilde{C}(U)$, is fairly close to unity throughout the magnetic-field range, indicating that SGM produces the wave function pattern independent of the transmission resonance. (The horizontal bars on the left-hand side in Fig. 2 show the respective values at $\hbar\omega_c/E_F=0.0065$, i.e., when the magnetic field is completely away from transmission resonances.) The correlation is negative when the magnetic field is around the resonance peak. When the magnetic field is set to values for the adjacent resonance dip of the pair, C suddenly turns to positive values. We will return to this point later. The dotted line in Fig. 2(a) shows the average of $|\delta G|$ within the cavity area depicted in Fig. 1(c), $\Delta G=\langle|\delta G|\rangle$. As the conductance is sensitive to the potential alteration at the resonance, ΔG increases exponentially at the transmission resonance.

We show in the inset of Fig. 2(b) the variation of the correlation when the amplitude U of the potential modulation is varied. (We do not show $\tilde{C}$ as $|C|\approx\tilde{C}$ at this magnetic field.) The correspondence between the SGM image and the pattern in LDOS deteriorates when the potential modulation is excessive. Nevertheless, given the slow deterioration, large values of U would be beneficial in experimental situations due to the strong enhancement of ΔG. The SGM image produces the scarlike pattern even when the bias potential is attractive $(U<0)$, as shown by the triangles. An attractive potential affects the wave function less effectively than a repulsive potential. The dominant influence of an attractive potential on the wave function is to increase its magnitude at the location of the potential. The enhancement is rather subtle compared to the suppression of the magnitude caused by a repulsive potential.[9] Therefore, ΔG is considerably smaller for $U<0$ than for $U>0$. Because of the gentle and locally contained influence of the perturbation, SGM reproduces the scarlike pattern with nearly complete fidelity for the attractive bias. (This advantage would probably be insignificant in experimental situations where the range of the potential "indentation" is likely to be larger than λ_F.)

In the experiment by Crook *et al.*,[3] scarlike features were observed to emerge while the magnetic field was varied. We point out a critical difference in the strength of the magnetic field in our simulations. As has been demonstrated in Ref. 12, a magnetic field realizes mixed dynamics, irrespective of the type of the underlying classical dynamics in the absence

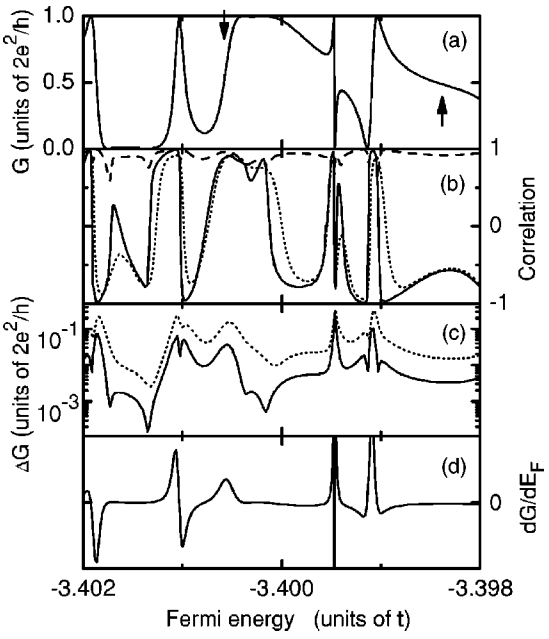

FIG. 3. (a) Magnetoconductance, (b) correlations C and $\tilde{C}$ (dashed line), and (c) magnitude of conductance change ΔG in a stadium cavity. The derivative dG/dE_F of the conductance curve is shown in (d). In (b) and (c), $U=0.1t$ and $0.5t$ for the solid and dotted lines, respectively. For $\tilde{C}$ in (b), $U=0.1t$. The arrows in (a) indicate the energies at which the plots in Fig. 4 are calculated.

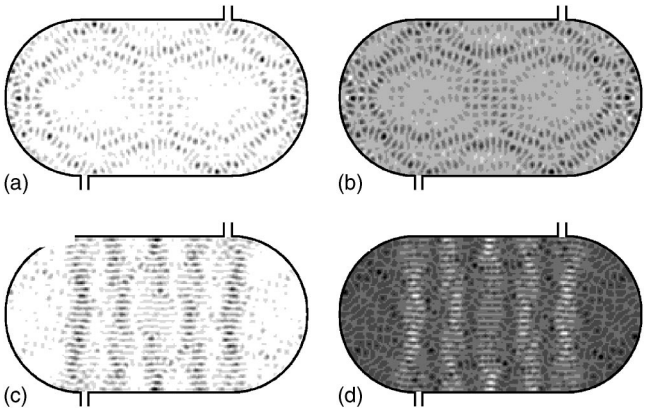

FIG. 4. Comparison between the local density-of-states $\rho(\mathbf{r})$ [(a) and (c)] and the images constructed by the potential-induced conductance change $\delta G(\mathbf{r})$ when $U=0.1t$ [(b) and (d)]. Fermi energy is $E_F=-3.4006t$ for (a) and (b) and $-3.3984t$ for (c) and (d). The black and white regions in the gray scale correspond, respectively, to $\delta G/(2e^2/h)\approx -0.32$ and 0.16 in (b) and -0.021 and 0.035 in (d). Darker regions represent larger ρ in (a) and (c).

of a magnetic field, when the diameter of the cyclotron orbit $l_c=2\hbar k_F/eB$, where $k_F=2\pi/\lambda_F$, is slightly larger than the cavity size. In Figs. 1 and 2, the magnetic field was thus chosen to be small. (The condition $l_c=W$ is fulfilled at $\hbar\omega_c/E_F\approx 0.045$ in our soft-wall cavity.) The high-resolution SGM images in the experiment[3] were taken when the ratio between l_c and the cavity size was ~ 2. The images were inevitably dominated by a stable orbit in such a circumstance.

We turn our attention to examining the SGM images obtained in chaotic quantum cavities. A standard method to establish chaotic dynamics is to shape the cavity to a stadium. In Fig. 3(a), we show the conductance of a stadium quantum cavity. To rule out the possibility of mixed dynamics being induced by a magnetic field, the Fermi energy is varied here when $B=0$. The widths of the stadium cavity are $100a$ and $200a$ in the narrow and wide directions, respectively. The width of the leads is $5a$. Only the lowest mode is occupied below the Fermi level in the leads. The correlation, C (solid and dotted lines) and $\tilde{C}$ (dashed line), and ΔG are shown in Figs. 3(b) and 3(c), respectively. One finds that $\tilde{C}$ is again approximately unity in the whole energy range. We show two examples of a comparison between the SGM images and LDOS in Fig. 4. The correspondence is remarkable. The scar pattern changes completely with a minor change of the cavity parameters, e.g., E_F in Fig. 4.[13] This sensitivity manifests the quantum-mechanical origin of the scar. The classical trajectories in chaotic cavities may be altered significantly by placing a probe-induced scattering potential. Nevertheless, as long as the conductance change serves as a measure of the extent of the alteration of the trajectories, the imaging of the scarred wave function in chaotic quantum cavities is accomplished by SGM. In experiments, however, the scarlike pattern due to stable orbits would be easier to observe than the scarred wave function in chaotic cavities as the nonuniformity is more pronounced in the former case than in the latter.

The abrupt change of C between nearly complete positive and negative correlations is found again at the transmission resonances. For an isolated transmission peak, C changes from ≈ 1 to ≈ -1 with increasing E_F, giving rise to an "N-shaped" characteristic. For a combination of a resonance peak and a resonance dip in the transmission, an "M"- or "W"-shaped characteristic is found, depending on the order the two transmission resonances are arranged in energy. This behavior can be understood as follows. The influence of a short-range "impurity" potential induced by the scanning probe is roughly to shift the conductance curve in energy (and in magnetic field).[9] Therefore, the conductance increases for energies on one side from the transmission resonance and decreases for energies on the other side. The overall response integrated in the cavity area would result in positive and negative correlation on each side of the resonance, giving rise to a change in the polarity of the correlation. The derivative of the conductance dG/dE_F plotted in Fig. 3(d) provides a satisfactory agreement with C.

In stadium cavities, electrons need to be bounced from the cavity boundary a large number of times in order for the classical dynamics to become fully chaotic. In an open system, the electrons may leave the cavity before the classical trajectories are sufficiently shuffled. The amplitude of conductance fluctuations has revealed that,[14] as a consequence, the underlying classical dynamics in open stadium cavities cannot be regarded as strictly chaotic, unless perhaps the leads are significantly narrow.[15,16] Therefore, we also utilize an alternative model for chaotic cavities in order to be certain about the underlying classical dynamics. It has been shown that short-range boundary disorder is extremely efficient in generating chaotic dynamics in a lattice model.[14,17] Figure

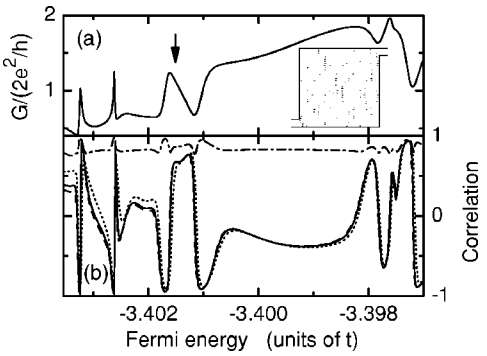

FIG. 5. (a) Conductance of a square quantum cavity having a short-range boundary disorder. The inset illustrates the cavity geometry together with the local density-of-states $\rho(\mathbf{r})$ at E_F indicated by the arrow. (b) Correlation C when $U=0.01t$ (dashed line), $0.1t$ (solid line), and $0.5t$ (dotted line). The correlation $\tilde{C}$ is shown by the dash-dotted line for $U=0.1t$.

5(a) shows the energy dependence of the conductance in a square cavity having a rough boundary. The cavity geometry is illustrated in the inset of Fig. 5(a). The width of the cavity is $161a$. The leads are $15a$ wide. Three modes are occupied below the Fermi level in the leads. The on-site energy of the boundary lattice sites of the cavity has been modified randomly by amounts distributed uniformly between $-d/2$ and $d/2$ ($d=t$ in Fig. 5).

The correlation C is shown in Fig. 5(b) for three values of the potential modulation U to carry out SGM. Similar to the observations for the other two types of quantum cavities that we have investigated above, $\tilde{C}$ is roughly unity, confirming that the scar in chaotic cavities can be indeed imaged by SGM. An interesting difference for the fully chaotic quantum cavity is that C depends only weakly on U despite that ΔG increases exponentially with U (not shown). The deterioration of the fidelity in the inset of Fig. 2(b) when the potential modulation is excessive is due primarily to the appearance of the ringlike distortion in the SGM images. Such a ring formation is an indication of the existence of spatial correlation in the scarlike feature, which is understandable as a specific stable orbit is responsible for the scarlike feature. The scar patterns in chaotic quantum cavities do not originate from specific orbits. This may imply that the response of the electronic state associated with the scar to a perturbation is short ranged. As a consequence, the ringlike distortion is practically absent in the SGM images of fully chaotic quantum cavities.

This work was supported in part by the Deutsche Forschungsgemeinschaft and by the NEDO collaboration program.

[1] M. A. Topinka, B. J. LeRoy, S. E. J. Shaw, E. J. Heller, R. M. Westervelt, K. D. Maranowski, and A. C. Gossard, Science **289**, 2323 (2000); M. T. Woodside and P. L. McEuen, *ibid.* **296**, 1098 (2002).
[2] T. Gramespacher and M. Büttiker, Phys. Rev. B **60**, 2375 (1999).
[3] R. Crook, C. G. Smith, A. C. Graham, I. Farrer, H. E. Beere, and D. A. Ritchie, Phys. Rev. Lett. **91**, 246803 (2003).
[4] L. Kaplan and E. J. Heller, Ann. Phys. (N.Y.) **264**, 171 (1998).
[5] G. M. Zaslavsky, M. Edelman, and B. A. Niyazov, Chaos **7**, 159 (1997).
[6] R. Ketzmerick, Phys. Rev. B **54**, 10841 (1996).
[7] O. Agam and S. Fishman, Phys. Rev. Lett. **73**, 806 (1994).
[8] M. Mendoza and P. A. Schulz, Phys. Rev. B **68**, 205302 (2003).
[9] Y. Takagaki and D. K. Ferry, Phys. Rev. B **45**, 6715 (1992).
[10] Y. Takagaki and K. H. Ploog, Phys. Rev. E **62**, 4804 (2000).
[11] L. Kaplan, Phys. Rev. Lett. **80**, 2582 (1998).
[12] Y. Takagaki, M. ElHassan, A. Shailos, C. Prasad, J. P. Bird, D. K. Ferry, K. H. Ploog, L.-H. Lin, N. Aoki, and Y. Ochiai, Phys. Rev. B **62**, 10255 (2000).
[13] W. E. Bies, L. Kaplan, M. R. Haggerty, and E. J. Heller, Phys. Rev. E **63**, 066214 (2001).
[14] Y. Takagaki and K. H. Ploog, Phys. Rev. B **64**, 245336 (2001).
[15] H. Alt, H. D. Gräf, H. L. Harney, R. Hofferbert, H. Rehfeld, A. Richter, and P. Schardt, Phys. Rev. E **53**, 2217 (1996).
[16] For this reason the width of the leads was reduced to sustain only the lowest mode in Figs. 3 and 4. The large values of $\tilde{C}$ in Fig. 3 for energies away from the transmission resonances and in Fig. 5, in which the leads are wide, indicate that the width of the leads does not influence the results.
[17] E. Cuevas, E. Louis, and J. A. Vergés, Phys. Rev. Lett. **77**, 1970 (1996).